Intra-oceanic emplacement of the Comoros Archipelago through inherited fracture zones

Charles Masquelet, Louise Watremez, Sylvie Leroy, Daniel Sauter, Matthias Delescluse, Nicolas Chamot-Rooke, Jean Claude Ringenbach, Isabelle Thinon, Anne Lemoine, Dieter Franke

Intra-oceanic emplacement of the Comoros Archipelago through inherited fracture zones

Charles Masquelet*1, Louise Watremez2, Sylvie Leroy1, Daniel Sauter3, Matthias Delescluse4, Nicolas Chamot-Rooke4, Jean Claude Ringenbach5, Isabelle Thinon6, Anne Lemoine6 and Dieter Franke7

1 Sorbonne Université, CNRS, Institut des Sciences de la Terre de Paris (ISTeP), Paris, France
2 Université de Lille, CNRS, Université Littoral Côte d'Opale, IRD, UMR 8187 – LOG – Laboratoire d'Océanologie et de Géosciences, Lille, France
3 Institut Terre et Environnement de Strasbourg (ITES), CNRS Université de Strasbourg, Strasbourg, France
4 Laboratoire de Géologie, CNRS UMR 8538, École normale supérieure, PSL University, Paris, France
5 TotalEnergies SE, CSTJF, Pau, France
6 Bureau de Recherches Géologiques et Minières (BRGM), Orléans, France
7 Bundesanstalt für Geowissenschaften und Rohstoffe (BGR), Hannover, Deutschland

*Corresponding author: charles.masquelet@sorbonne-universite.fr
Sorbonne Université, CNRS, Institut des Sciences de la Terre de Paris (ISTeP), 4 place Jussieu, Paris, France

Highlights:

- The crust of the Comoros Basin is oceanic, resolving past controversies
- Basement roughness is typical of intermediate-spreading ridges
- Unloaded basement depth matches Cretaceous or Jurassic oceanic lithosphere
- Comoros volcanic islands emplaced through re-activated fracture zones
- The Comoros Archipelago aligns with a change in the direction of the fracture zones

Abstract

We shed light on the nature and structure of the crust surrounding the Comoros Archipelago, western Indian Ocean, offering insights into the region's geological history and volcanic island formation. Our comprehensive study encompasses the acquisition of new, deeply penetrating seismic data from the SISMAORE cruise (refraction and reflection seismic), and the subsequent analysis of the characteristics and structure of the crust surrounding the Comoros Archipelago. Both the reflection seismic imaging and the velocity structure using ocean bottom seismometers indicate that the crust of the Comoros Basin crust exhibits oceanic characteristics, thus resolving previous controversies about its nature. The thickness of the oceanic crust ranges from 5.8-6.6 km in the north of the archipelago to 6-7.2 km within the Comoros Basin. The estimated roughness of the top basement in the Comoros Basin ranges from 110 to 200 m values typical of intermediate spreading ridges, such as the extinct spreading centre in the West Somali Basin.

The unloaded basement depth of the Comoros Basin closely matches the expected water-loaded subsidence for a Cretaceous or Jurassic oceanic lithosphere. In contrast, the West Somali Basin to the north of the Comoros Archipelago has shallower basement depths, potentially linked to recent volcanic activity along the archipelago. We propose that the pre-existing oceanic fracture zones in the West Somali Basin underwent reactivation, first during the Turonian period and later during the Late Eocene. These reactivated fracture zones may have acted as preferred pathways for the emplacement of the volcanic islands of the Comoros Archipelago. The EW trend of the archipelago appears to follow a marked change in the direction of these reactivated fracture zones, suggesting that the associated lithospheric weakening likely played a critical role in facilitating the formation of the Comoros Archipelago.

1. Introduction

The origin of the Comoros Archipelago (Fig. 1), in the northern Mozambique Channel, has been the subject of lively debate for some fifty years. It has long been interpreted as being due to the impingement of a mantle plume beneath a moving oceanic lithosphere (Emerick and Duncan, 1982; Hajash and Armstrong, 1972). While hotspot volcanism may be supported by the enriched mantle signature of the lavas on Grande Comore Island (Class et al., 2009), the general E-W trend of the Comoros

Archipelago is not consistent with the northward absolute motion of the Somalia plate (Morgan and Morgan, 2007).

In May 2018, a major phase of seismo-volcanic activity gave birth to the large – 820 m high and 5 km in diameter - submarine Fani Maoré volcano, sitting at about 3500 m water depth, east of Mayotte Island (Feuillet et al., 2021; Lemoine et al., 2020; Masquelet et al., 2022; Thinon et al., 2022). The present-day active volcanism both on Grande Comore Island and east of Mayotte Island together with widespread Holocene volcanic activity on Anjouan, Mohéli, and Mayotte Islands (Quidelleur et al., 2022; Rusquet et al., 2023) does not support a simple model of punctual and vertically rising mantle plume material piercing a moving lithosphere.

The recent seismo-volcanic crisis east of Mayotte Island together with previous sparse focal mechanisms along the Comoros Archipelago suggest mainly strike-slip faulting with a NE-SW normal component (Feuillet et al., 2021; Lemoine et al., 2020). This seismicity has been interpreted as resulting from a nascent plate boundary between the Somalia and Lwandle plates connecting the East African Rift System (EARS) to the Tertiary-Quaternary volcanism and rifting of Madagascar (e.g. (Famin et al., 2020; Feuillet et al., 2021; Thinon et al., 2022). However, there is no consensus over the offshore extent of the EARS. The deformation identified onshore and on the seafloor, is thought to be either focused within a 150-200 km-wide right-lateral shear zone along the Comoros Archipelago (Famin et al., 2020; Feuillet et al., 2021; Thinon et al., 2022) or distributed within a ~600-km-wide deformation zone positioned between the Rovuma microplate and the Somalian plate that extends over large parts of Madagascar and the Comoros islands (Stamps et al., 2021).

Although crucial to understanding the origin of the archipelago, the nature of the crust beneath the Comoros volcanic islands and in the Comoros Basin, between the archipelago and Madagascar, is poorly known. Fundamentally different interpretations have been issued. Oceanic crust, continental crust and a wide continent-ocean transition have been proposed for the Comoros Basin e.g. (Coffin et al., 1986; Lort et al., 1979; Nougier et al., 1986). In this paper, we first briefly review these interpretations, then present our newly collected seismic data set, show our results on the oceanic nature and structure of the crust around the Comoros Archipelago and finally discuss the implications of our findings for the emplacement of the magma that formed the Comoros volcanic islands. We show that the location of the islands is

controlled by the pre-existing segmentation of the oceanic crust of the West Somali Basin.

2. Geological Background

North of the Comoros Archipelago, magnetic anomalies related to the spreading ridge of the West Somali Basin argue for a typical oceanic lithosphere e.g. (Cochran, 1988; Davis et al., 2016; Sauter et al., 2016; Ségoufin and Patriat, 1980). There, magnetic anomalies, from M24 (~152 Ma, according to the time scale of Ogg, (2020)) to M0 (~121 Ma) indicate slow to intermediate spreading rates (~30 to ~60 km/Ma full rates) until Aptian time when spreading ceased in the West Somali Basin (Davis et al., 2016). The nature of the crust south of the archipelago is less clear. Rabinowitz et al. (1983) interpreted magnetic anomalies up to the M25 magnetic anomaly (~153 Ma), while Davis et al. (2016) and Cochran (1988) were unable to correlate any significant magnetic anomalies on a few magnetic profiles. From an early sonobuoy experiment using only two instruments, Lort et al. (1979) speculated that the Comoros Archipelago marks the boundary between oceanic crust to the north and continental crust to the south. Later, with over a hundred sonobuoy records, Coffin et al. (1986) showed that both the West Somali and Comoros basins are oceanic in character.

However, the observation of sandstone xenoliths in Comoros lavas (Flower and Strong, 1969) and the presence of a km-scale quartzite massif on Anjouan Island have been used to suggest that the archipelago may be built on stretched continental crust (Montaggioni and Nougier, 1981). It was further proposed that magmatism along the Comoros Archipelago is controlled by deep lithospheric faults, linked to an inferred wide continent-ocean transition (Nougier et al., 1986; Tzevahirtzian et al., 2021).

Based on a single receiver function analysis at Mayotte Island, Dofal et al. (2021) proposed a continental nature of the crust beneath Mayotte. However, from a combined analysis of receiver functions and the joint inversion of receiver function and Rayleigh wave dispersion data, Dofal et al. (2023) could not discriminate the oceanic or continental nature of the crust beneath Mayotte Island. Recently, Roche and Ringenbach (2022) used seismic reflection profiles to show that oceanic crust is present at 13.5°S, to the southwest of Moheli Island. Wide-angle seismic data also showed the presence of oceanic crust on the eastern flank of the Davie Ridge, at 14.5°S (Vormann et al., 2020; Vormann and Jokat, 2021).

The seismic stratigraphy of the Comoros and Somalia basins is based on the relatively well-known stratigraphy of the northern Mozambique Channel and the West Somali Basin (Coffin and Rabinowitz, 1992; Franke et al., 2015; Mahanjane, 2014; Mougenot et al., 1986; Roche and Ringenbach, 2022). Using IODP Site 1476 and DSDP Site 242 (Hall et al., 2017; Simpson et al., 1974) located on the Davie Ridge at the northern entrance of the Mozambique Channel, and seismic reflection profiles that intersect these sites, Masquelet (2023) and Masquelet et al.(submitted) identified the top Miocene and top Oligocene horizons (TM and TO in Fig. 3). These horizons were further extended towards the Comoros Archipelago, 500 km away. They also identified the Cretaceous-Paleogene unconformity (K/Pg, Fig. 3), which appears as a prominent event in the seismic profiles across the West Somali Basin and offshore Majunga Basin (Franke et al., 2015; Leroux et al., 2020; Mahanjane, 2014). They also interpreted the package of high amplitude and low frequency discontinuous reflectors beneath the K/Pg reflector as the Turonian volcanism previously observed in the Diego and Majunga basins offshore Madagascar (Coffin and Rabinowitz, 1992; Leroux et al., 2020).

3. Data acquisition and processing

A regional-scale acquisition of geophysical and geological data was conducted off the Comoros Archipelago aboard the R/V Pourquoi pas? in 2021 (Fig. 1), (SISMAORE cruise, Thinon et al., 2022, 2020). 1480 km of deep multichannel seismic reflection data (960 channels) and 6800 km of shallow seismic reflection profiles (48 channels) were acquired. In addition, three OBS (Ocean-Bottom Seismometers) recorded the seismic shots along the multichannel line M01 high-resolution profile, located East of Mayotte (Fig. 1C). Published seismic reflection profiles within the Comoros Basin complement this new data set (Fig. 1). We also incorporated the seismic reflection profiles of the R/V Sonne SO-231 cruise (Franke et al., 2015; Klimke et al., 2016) and the R/V L'Atalante PTOLEMEE cruise (Jorry, 2014; Leroux et al., 2020). We also used ION Geophysical™ seismic multichannel lines partly published by Leroux et al. (2020), Sinha et al. (2019), and Roche and Ringenbach (2022) on the eastern flank of the Davie Ridge and in the Comoros Basin.

3.1. Long-streamer 960-channel seismic reflection profiles

We collected a set of 12 multichannel seismic (MCS) profiles (6000 m long streamer with 960 channels spaced every 6.25 m). The seismic source consisted of 16 airguns triggered every 40 s with a total volume of ~82 L (4990 cu. in.). The record length was 20 s with a sampling rate of 2 ms. The distance between each common depth point (CDP) is 3.25 m. Super gather CDPs were built by merging four CDPs in a bin of 12.5 m during processing, allowing for a fold of 60. Processing involved a typical workflow using CGG GeoVation® software in the pre-stack domain (including trace editing, amplitude correction, normal move-out correction, FK-filtering, multiple attenuation, and predictive deconvolution). Masquelet et al. (2022), Masquelet (2024), Masquelet et al. (submitted) describe in detail the seismic processing of this data set.

3.2. Short-streamer 48-channel seismic reflection profiles

A series of 110 48-channel seismic reflection profiles was collected using a 600 m-long streamer (channels spaced every 6.25 m). The source consisted of two airguns with a total volume of 4.91 L (300 cu. In) firing every 50 m (recording length of 9 s and inter CDP is 3.125 m). CGG GeoVation® software was used for standard processing including 12.5 m binning (6-fold by stacking 2 adjoining traces), NMO correction, stack and a Kirchhoff migration at 1500 m/s.

3.3. OBS data set

A set of three OBSs recorded the shots during the acquisition of the 960 channel seismic reflection profiles (Fig. 1C). These three instruments were deployed along the ~290 km long M01 line, which is located east of Mayotte with a SSW-NNE orientation and crosses the new Fani Maoré volcano (Masquelet et al., 2022). The OBSs also recorded shots along cross lines, allowing the estimation of seismic velocities along different azimuths.

After clock-drift correction, the instruments were relocated using the direct wave picks from the shots within 10 km of their deployment location, the bathymetric grid, and averaged seismic velocities in the water column (1.505 km/s). The OBS records, organized as receiver gathers, allowed the picking of arrival times of several seismic phases in the different geological layers down to the uppermost mantle (Appendices A and B). We used a forward modelling program, RAYINVR (Zelt and Smith, 1992), following a top-down layer stripping strategy to generate velocity models that reproduce the picked data within their uncertainty range (Appendix C). We modelled 2

or 3 lines for each instrument. Here we present the velocity model along M01, which crosses all 3 instruments, although each instrument can be considered as an independent ~1D model since no seismic ray crosses the entire model (Fig. 2A). This issue implies that the obtained velocities and thicknesses may not be so well constrained, but this is counterbalanced by the use of strong constraints from the coincident high-resolution seismic reflection data. The initial velocity model was built using the picks at the main geological interfaces, where available, and a first estimate of (1) the interval velocities in the sediments along these seismic reflection profiles and (2) the apparent velocities of the corresponding refracted arrivals on the OBS records used to convert these interfaces from two-way travel-time to depth. RAYINVR modelling allows us to compute synthetic arrival times from ray-tracing through the model, which we updated to reduce the misfit between computed and picked arrivals (Appendix C). The final model is converted to two-way travel time to allow for a comparison with coincident seismic reflection data (Fig. 2B). The vertical velocity profiles (Fig. 2C) provide an assessment of the robustness of the velocity models. It is noteworthy that a vintage sonobuoy profile (Lort et al., 1979) located only 7 km away from the OBS3 shows comparable velocities in the sediment layers but is limited to the top of the crust (Fig. 2C).

4. Results

The internal reflectivity of the crust imaged by seismic reflection shows a typical oceanic crustal layering as defined by the 1972 Penrose Conference (Fig. 4) (Bécel et al., 2015; Mutter and Carton, 2013; Sauter et al., 2021). It includes, from top to bottom, the following successive seismic facies: (1) a reflective top of basement with some short reflections in the shallowest part of the crust, (2) a transparent unit in the upper crust, (3) a more reflective lower crust with dipping structures and (4) a series of horizontal reflectors typically interpreted as the oceanic Moho, although various geological structures at the base of the crust may generate high-amplitude reflections (e.g. Collins et al., (1986)). We identified the seafloor multiple of the profile during the processing and took care of attenuating it using a demultiplex routine that filtered out low-velocity reflectors (i.e., velocities typical of shallow sediment layers rather than velocities expected near the Moho discontinuity). In addition, the velocity model requires two velocity gradients: a moderate velocity gradient below the basement and a low-velocity gradient above the Moho. We have therefore ensured that all the

reflectors at the base of the crust do not come from a multiple of the seafloor. This interpretation is confirmed by the OBS analysis, where geological layers were imaged down to the Moho or upper-most mantle (Fig. 2).

4.1. Nature of the crust in the Comoros Basin

Both seismic reflection and refraction (OBS) data show evidence for the presence of oceanic crust south and SE of Mayotte (Figs. 4 and 5). Seismic reflection data show oceanic Moho reflections that are roughly parallel to the top of the crust (at tens of kilometres scale, Fig. 4). The oceanic Moho is generally characterized by a few strong and continuous reflectors (Fig. 4 A&B) at about 9.5 s TWTT. However, a package of laterally discontinuous reflectors up to 0.25 s TWTT thick can also be observed locally (Fig. 4C). It may also be faint or absent, especially towards the volcanic islands or submarine volcanic provinces of the Comoros Archipelago postdating the emplacement of the oceanic crust.

The results obtained from the OBS data support the interpretation of the oceanic nature of the crust. Indeed, the velocity models obtained for the three OBSs show a clear 2-layer basement, with velocities that are typical for the oceanic crust (Fig. 5). The uppermost basement layer shows velocities ranging from 5.25 to 6.70 km/s and strong vertical velocity gradients (0.3-0.55 s^{-1}), which correspond to seismic velocities in basalts, i.e., the oceanic Layer 2. The lower crustal layer shows higher velocities (6.75-7.2 km/s) with lower velocity gradient (~0.1 s^{-1}), typical of the gabbroic oceanic Layer 3 (Fig. 5). More than 700 wide-angle reflected arrivals were picked at the interface between Oceanic Layer 2 and Layer 3, and almost 2,300 at the Moho, thanks to the fact that incidence angle is much wider than in seismic reflection data (near-critical reflections, see modelling statistics for phases 6.2 and 7.2, respectively, in Appendix C).

The nature of the crust around the Comoros Archipelago has been debated, including around OBS3. Fig. 5A shows a comparison of crustal velocities beneath OBS3 with values reported in the literature. Lort et al. (1979) speculated that the crust might be continental based on velocities down to the top basement, whereas our study provides information down to the uppermost mantle. It is now clear that we observe a typical oceanic layering (Fig. 5A; White et al. (1992)). Indeed, the continental-type velocities for the extended crust are much lower than in the crust under OBS3 (Fig. 5A; Christensen and Mooney (1995)). It has also been discussed whether the area

between the Madagascar margin and the ocean might be transitional (Nougier et al., 1986). Comparison with continental (Dean et al., 2000), and oceanic exhumed mantle zones (Van Avendonk et al., 2006)(Fig. 5A) shows that the lower crustal velocities beneath OBS3 are too slow to be consistent with a partially serpentinized mantle.

4.2. Thickness of the crust

We picked the top of the basement and the base of the crust to obtain the crustal thickness at places where the oceanic Moho is well marked by a series of highly reflective reflectors (Fig. 4). We then converted this TWTT thickness to kilometres using an average velocity of 6.56 km/s, which corresponds to the average seismic velocities we found for the crust from our OBS analysis.

Appendix D provides examples of crustal thickness measurements to the north (Table D1) and south (Table D2) of the Comoros Archipelago. Crustal thicknesses range from 1.8 to 2.07 s TWTT (5.9-6.8 km) north of Grande Comore. The crust is somewhat thicker in the Comoros Basin, ranging from 1.95 to 2.25 s TWTT (6.4-7.4 km) (see for example Fig. 3). This is consistent with our results from the OBS analysis in the Comoros Basin, which show a ~6.5-7 km thick crust beneath OBS3 and OBS2.

However, the crust is much thinner (~5 km) below OBS1 at the northern end of the profile. Velocity modelling shows that the thickness of the oceanic Layer 2 is homogeneously ~2-2.5 km, while the thickness of Layer 3 varies from ~2.5 km below OBS1 in the North to 4-5 km below OBS2 and OBS3 in the south (Fig. 5).

5.3 Top of the oceanic crust

5.3.1 Small-scale oceanic crust roughness

The variation of oceanic basement roughness at mid-oceanic ridges is primarily related to the spreading rate, which mainly controls the thermal state of the lithosphere (Goff et al., 1997; Sauter et al., 2018b). Estimating the roughness of the oceanic crust (i.e. the root mean square deviation of the residual basement relief) can thus provide insight into the spreading processes within the West Somali and Comoros basins. We selected three seismic reflection profiles in line with the inferred spreading direction to estimate the roughness of the oceanic crust. After removing the NS regional deepening of the basement, we obtained roughness values ranging from 110 to 200 m for the abyssal hill bathymetry along the three profiles (Fig. 6). Such roughness values are

typical for slow to intermediate spreading ridges (Goff et al., 1997; Sauter et al., 2018b) (Fig. 6).

5.3.2 Regional depth variation of the top oceanic crust

Mapping the basement depth along each seismic reflection profile (Fig. 7), we found that the top basement is much deeper in the Comoros Basin (mean depth of 7 km) than in the West Somali Basin to the north of the Archipelago (mean depth of 6 km). Using the sediment thickness derived from the seismic profiles and a conservative range for their mean density (2.0 to 2.2), the unloaded basement depth would be 5.4 km for the Comoros Basin and 5.0 km for the region north of the Archipelago (Fig. 8). Despite the large uncertainties inherent in such calculations, the unloaded depth in the Comoros Basin is not far from the asymptotic water-loaded subsidence inferred by Stein and Stein in their GDH1 plate cooling model (5560 m; Stein and Stein (1992)) (Fig. 8). Subsidence in the Comoros Basin is thus compatible with a Cretaceous or Jurassic age for the oceanic lithosphere. The West Somali Basin, north of the Archipelago, appears to be several hundred meters shallower (Fig.8). Seismic profiles image a rather sharp step in the topography of the top basement between 12.2°S and 12.5°S, along an EW trending line through the Comoros Archipelago joining Mohéli Island and Zélée Geyser banks (Figs 7 and 8). This shallower basement extends over a broad region, suggesting anomalous heating at mantle depth, possibly related to the recent volcanism discovered in the Mwezi and N'Droundé provinces to the northeast of Anjouan and Grande Comore islands and throughout the Comoros Archipelago (Rusquet et al., 2023; Thinon et al., 2022).

5.4 Compressional structures

Seismic profiles north of the Comoros archipelago document two distinct phases of compressional deformation. The first is Turonian in age and the second is Late Eocene.

The oldest event is recorded in the deepest sedimentary layers as a small dome bounded by reverse faults of opposite vergence (Figures 9 and 10). The dome is sealed by post-Turonian sediments, indicating an early phase of deformation. The basement faults are poorly imaged, but the sedimentary dome clearly coincides with a crustal basin of similar dimensions, suggesting tectonic inversion along basin-bounding faults (FZ1 in Fig. 9). Similar basins observed along the M02 profile (FZ2a

and b in Figs. 9 and 10) can be traced further north in the seismic lines (Fig. 10). They systematically correspond to elongated NNW-SSE trending gravity lows in the satellite-derived free-air gravity anomaly (Fig. 9) and are therefore interpreted as transform faults or fracture zones valleys that formed at the extinct seafloor spreading centre of the West Somali Basin (Davis et al., 2016) and were later reactivated.

The most recent event is associated with stronger compressional features that are well imaged north of Grande Comore Island along two intersecting EW and NS seismic profiles. The main episode of deformation is marked by a dense network of inverse faults in both the sedimentary cover and the crust. Oligocene sediments seal these structures. The amplitude of the uplifted areas reaches 0.3-0.4 s TWTT (300-400 m with an interval velocity of 2 km/s). The EW trending profile shows a series of strong reflectors occurring ~1 s below the top of the basement, all located beneath the uplifted area and a former small basin within the crust. These reflectors connect the oceanic Moho both east and west of the deformed area. We thus interpret them as corresponding to the deformed oceanic Moho. The thin crust beneath the uplifted area is of the type typically observed at transform faults near their intersection with oceanic ridge segments. Both the top basement and the Moho are shallower to the east of the deformed area than to the west, which may indicate a younger-aged oceanic lithospheric compartment to the east, suggesting that the profile crosses a fracture zone. Note that the Turonian phase is also observed in the easternmost part of this EW profile with a small doming of the early sediments (Fig.11A).

Both the Turonian and Oligocene compressive events thus appear to have overprinted the original network of transform faults and fracture zones inherited from the paleo-spreading centre of the West Somali Basin. Since some small faults reach the seafloor, we further propose that such reactivation may have continued until recent times. Compressive structures show several strong reflectors within the crust above the oceanic Moho and locally within the uplifted area (Fig. 11 B). We interpret these reflectors as indicative of magma intrusions along faults, typically found in the lower oceanic crust (Sauter et al., 2021) and possibly up to the seafloor. As magma is unlikely to be present 120 Ma after the cessation of the spreading, these intrusions are more likely to be related to the active magmatic province around the Comoros Archipelago, which would then extend 200 km further north than previously mapped (Thinon et al., 2022; Tzevahirtzian et al., 2021).

5. Discussion

5.1. Nature of the Comoros Basin

We found evidence for oceanic crust in the Comoros Basin, consistent with previous studies (Coffin et al., 1986), and have thus resolved past controversies about the nature of the crust around the Comoros Archipelago.

The Moho seismic reflection is weak in some parts of the study area. This is not surprizing, as there are many places, away from the axis of the mid-oceanic ridges, where the crust-mantle transition shows no distinguishable reflection (Mutter and Carton, 2013). Either the Moho interface is highly variable in structure, resulting in a gradual transition zone that is broad enough not to produce a vertical incidence response, and/or the scattering and attenuation properties in the crustal section lead to variable imaging conditions at the Moho level (Mutter and Carton, 2013). In our survey area, volcanic overprinting enhances the variability of both the sedimentary cover and the crustal structure (Masquelet et al., 2022). Locally absent Moho reflections have also been noted in the northern part of the West Somali Basin, where the variable seismic signature of the base of the crust has been attributed to faulting, deformation and/or intrusions (Sauter et al., 2018a; Sinha et al., 2019). Furthermore, no evidence for a clear oceanic Moho reflection was reported by Klimke et al. (2016) east of the Davie Ridge, where oceanic crust is inferred from wide-angle data (Vormann et al., 2020; Vormann and Jokat, 2021).

Because our data set does not include profiles right across the islands, we cannot rule out the possibility of some isolated continental blocks below the Comoros Islands, as has been hypothesized beneath some volcanic islands surrounded by oceanic crust such as Iceland or Mauritius (Foulger et al., 2020). Our dataset further shows that the young Fani Maoré volcano, which crowns the Mayotte volcanic edifice 50 km to the east of Mayotte Island, does not sit directly on the top of the basement but on a >2 km thick sedimentary unit above the oceanic crust (Masquelet et al., 2022). We conclude that such continental blocks, if present beneath the islands of the archipelago, would be of very small extent (<30-40 km) which seems unlikely when compared to typical microcontinents such as the undisputed examples of Jan Mayen and the Seychelles (Péron-Pinvidic and Manatschal, 2010).

The obtained 6-7 km crustal thicknesses in the Comoros Basin are in agreement with the 6.72 km average thickness for oceanic crust >125 Ma old (Christeson et al., 2019). Similar crustal thicknesses have been obtained from both seismic reflection

profiles and wide-angle seismic data on the eastern flank of the Davie Ridge between 13.5 and 14.5°S (Roche and Ringenbach, 2022; Vormann et al., 2020; Vormann and Jokat, 2021). This range of thickness, together with the estimated roughness of the top basement (110-200 m), is typical for spreading ridges with a relatively high magmatic budget and minor contribution from tectonism (Goff et al., 1997). This also agrees with the intermediate spreading rate indicated by the magnetic anomalies for the extinct spreading centre of the West Somali Basin (Davis et al., 2016).

Locally the crust may be much thinner (e.g. ~5 km below OBS1). The velocity models show that while the oceanic layer 2 does not change along the M01 profile, Layer 3 is ~2 km thinner below OBS1. Because a thinner Layer 3 is often observed at the segment ends of slow to intermediate spreading ridges e.g. (Minshull et al., 2006), this variation in Layer 3 thickness may indicate the presence of a fracture zone at the northern end of the M01 profile, beneath OBS1. We note that the top of the crust along the M01 profile is shallowing northward with two topographic steps between OBS3 and OBS2 and below OBS1 separating sections of more or less constant depth (Fig. 2). We interpret this stepwise depth variation as indicating successive sections of oceanic lithosphere of different ages and thus the presence of fracture zones that offset segments of the extinct spreading ridge of the West Somali Basin. Moreover, a basin is well imaged beneath OBS1 on profile M02, which also corresponds to a gravity lineament revealing the paleo-segmentation of the extinct spreading centre (Figs. 9 and 10). Some of these fracture zones have been locally reactivated.

5.2. Pre-existing structures in the Comoros and West Somali Basins and emplacement of the Comoros Archipelago

Both reactivation of NS tectonic features and volcanic activity occurred along the Davie Ridge in the Late Cretaceous after the cessation of the southward drift of Madagascar (Bassias and Leclaire, 1990; Mascle et al., 1987). Reactivation of former extensional faults has also been documented for the onshore and offshore Majunga Basin during the Late Cretaceous (Razafindrazaka et al., 1999). Transpressional events have also been evidenced from the Late Cretaceous to the Paleogene along other NS-trending major fracture zones close to the East African margin, such as the Seagap (offshore central Tanzania) and Walu faults (i.e. the northern extension of the Davie Ridge (Roche and Ringenbach, 2022). Here we show that such a reactivated

fracture zone is also observed in the Late Eocene north of the Comoros Archipelago, away from these major transform faults.

Several islands of the archipelago, such as Grande Comore, Anjouan and Mayotte, show an elongated shape, several rift zones, numerous dikes and alignments of offshore volcanoes with a main NS to NNW-SSE orientation, along with some minor orientations (Famin et al., 2020) (Fig. 12). Similarly, the recently discovered N'droundé Ridge province (see Fig. 1 for location) and the Domoni ridge between Grande Comore and Mohélie islands show the same ~NS orientation (Thinon et al., 2022). (Famin et al., 2020) showed that the maximum horizontal stresses of the paleostress tensors obtained from fault analysis at Mayotte, Anjouan and Mohéli islands are consistently oriented NNW-SSE. We also note that several post-seafloor-spreading volcanic edifices of Late Cretaceous age have been found aligned with fracture zones of the extinct spreading centre both in the northern part of the West Somali Basin (Cruciani and Barchi, 2016) and on the eastern flank of the Davie Ridge (Klimke et al., 2016). It has also been suggested that deep lithospheric melt was channelized along shear zones up to shallow deformation corridors to feed volcanic edifices along pre-existing oceanic fracture zones of the West Somali Basin (Sauter et al., 2018a). We therefore propose that the emplacement of the volcanic edifices of the Comoros Archipelago is partly controlled by mechanically weak zones along pre-existing fracture zones of the oceanic crust.

Several analyses of the satellite-derived gravity data have resulted in maps of gravity lineaments related to fracture zones, all of which show a change in spreading direction at about 12°S from NW-SE to the south, to NS in the West Somali Basin (Davis et al., 2016; Phethean et al., 2016; Reeves, 2018; Sauter et al., 2018a) (Fig. 12). We note that the oceanic crust is thinner north of the archipelago and thicker south, and that the depth of the oceanic basement is shallower in the north than in the south (Fig. 7). The different thicknesses and depths could indicate a change in the magma budget related to the change of spreading direction. This change is also well defined by the striking bend in the Davie Ridge at 12-14°S, which shows diffuse extension compared to more focused extension further north and south, in the Kerimba and Lacerda Miocene to Pliocene narrow grabens, respectively (Franke et al., 2015) (Fig. 10). The islands of the Comoros Archipelago show a general EW alignment at the same latitude (12-13°S) with NS gravity lineaments to the north and NW-SE ones to the south (Fig. 12). We compare this geodynamic context with the so-called Buried

Hills in southeastern Sri Lanka. These magmatic structures form an elongated NE-SW trending chain between the NS-oriented 85°E Ridge and the Afanasy Nikitin Seamounts (Altenbernd et al., 2020). They are located at a border between swaths of oceanic crust formed by seafloor spreading in two different directions. It was thus suggested that they may have been set up along a line of pre-existing structural weakness (Altenbernd et al., 2020). Reactivation of oceanic fracture zones has also been inferred to explain the formation of the Bathymetrists seamounts in the Central Atlantic (Van Der Zwan et al., 2023). There, a change in the motion of the African plate 60-40 Ma ago, together with the reactivation of the fracture zones of the strongly sheared Equatorial Atlantic, created pathways in the lithosphere and possibly enhanced magmatism (Van der Zwan et al., 2023). We thus suggest that the segmentation of the extinct spreading centre of the West Somali Basin strongly controls the emplacement of the Comoros Archipelago. This does not exclude other controlling mechanisms, such as those suggesting a nascent plate boundary between the Lwandle and Somalia plates (Famin et al., 2020; Feuillet et al., 2021). The Late Eocene reactivation phase, coeval with the onset of the Arabia-Eurasia collision at the Eocene/Oligocene boundary (Song et al., 2023), may have triggered the weakening of the fracture zones in the Somali and Comoros basins. This phase would then result in the emplacement of volcanic edifices along a weakened area where these fracture zones change direction, favouring a nascent plate boundary.

6. Conclusions

1) The crust of the Comoros Basin is decidedly oceanic in character resolving controversies of the past.
2) The crust is thinner (5.76-6.62 km) north of the Archipelago and thicker (6-7.2 km) in the Comoros Basin and has a top basement roughness of 110-200 m. Such crustal thickness and top basement roughness are typical of crust formed at intermediate spreading ridges such as the extinct spreading centre of the West Somali Basin.
3) The unloaded basement depth of the Comoros Basin closely matches the asymptotic subsidence predicted by the Stein and Stein (1992) plate cooling model, indicating a possible Cretaceous or Jurassic age for the oceanic lithosphere. The West Somali Basin north of the archipelago appears to have

a shallower basement, possibly linked to anomalous mantle heating associated with recent volcanism in the Mwezi and N'Drounde provinces northeast of Anjouan and Grande Comore islands, respectively.

4) The pre-existing fracture zones of the extinct spreading centre of the West Somali Basin have been reactivated first in Turonian time and then in Late Eocene time. They may have served as mechanically weak zones controlling the emplacement of the volcanic islands of the Comoros Archipelago.
5) We suggest that the weakened area formed by the alignment of changes in direction of these fracture zones may have favoured the emplacement of the Comoros Archipelago.

Acknowledgements

This paper is a contribution of the COYOTES and SISMAORE teams (http://www.geocean.net/coyotes/doku.php?id=start). The processing and the detailed analysis of these geophysical and geological data are mainly carried out in the framework of the ANR COYOTES (ANR-19-CE31-0018, https://anr.fr/Projet-ANR-19-CE31-0018) project funded by the French ANR (Agence Nationale de Recherche) and the BRGM. The SISMAORE cruise was mainly funded by the Flotte Océanographique Française (French Oceanographic Fleet) and the BRGM. We thank CGG for allowing us to use the CGG GeoVation software in the CNRS laboratories. We thank Captains P. Moimeaux and G. Ferrand, the crews, and the technicians from the R/V Pourquoi Pas? (FOF by IFREMER/GENAVIR). Thanks to the BRGM regional department of Mayotte. Thanks to REVOSIMA and DIRMOM for their assistance with the cruise during the COVID sanitary crisis. OBS facilities are from the IPGP instrumental network. Masquelet's Ph.D. was funded by the Sorbonne Université through the ANR COYOTES. We thank TotalEnergies and TGS for permission to use some of their seismic reflection profiles.

Figure captions

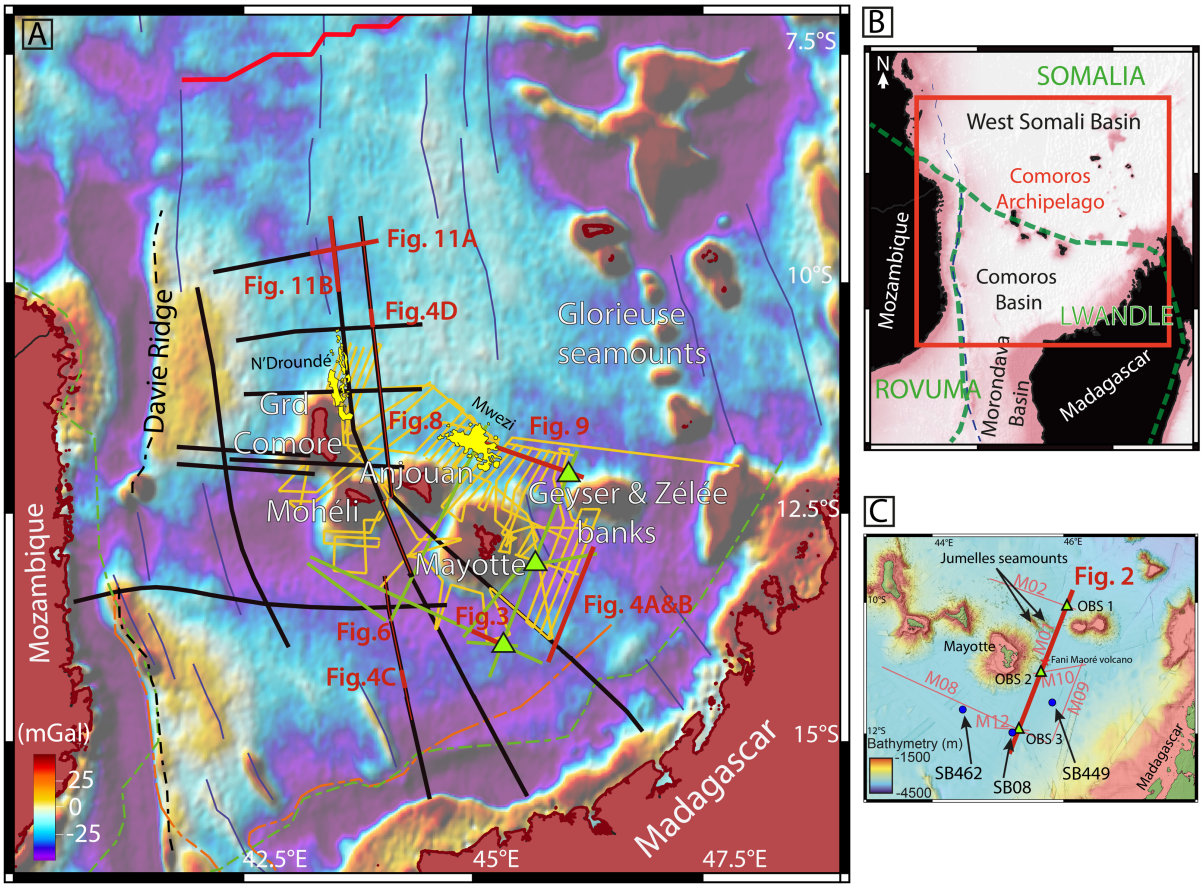

Figure 1: Map of the study area offshore the Comoros archipelago (A). Orange lines indicate the 48-channel seismic reflection profiles and green lines show the 960-channel seismic reflection profiles collected during the SISMAORE cruise (Thinon et al 2020). Black lines indicate the TGS lines available for the study. The green triangles indicate the location of the OBSs (ocean bottom seismometers) of the SISMAORE cruise. The N'Droundé and Mwezi volcanic provinces are shown in yellow. The blue lines correspond to the fracture zones of Davis et al. (2016). The green and orange dashed lines correspond to the COB (Continent-Ocean Boundary) of Roche and Ringenbach (2022) and Sinha et al. (2019), respectively. The black dashed line corresponds to the Davie Ridge. Thick red lines indicate the part of the profiles shown in the following figures of this paper. The background image is the satellite-derived free air gravity anomaly grid of Sandwell et al. (2014); (B) Location of the study area in the western Indian Ocean. The dashed green lines indicate the inferred plate boundaries after Michon et al. (2022); (C) Location of the OBSs of the SISMAORE cruise (green triangles) and the sonobuoys SB08 of Lort et al. (1979) and V449 of Coffin et al. (1986)

(blue points). The numbering of the seismic reflection profiles (M01, M08 etc…) is also indicated. The background bathymetric grid is a compilation of several cruises after Masquelet et al. (submitted).

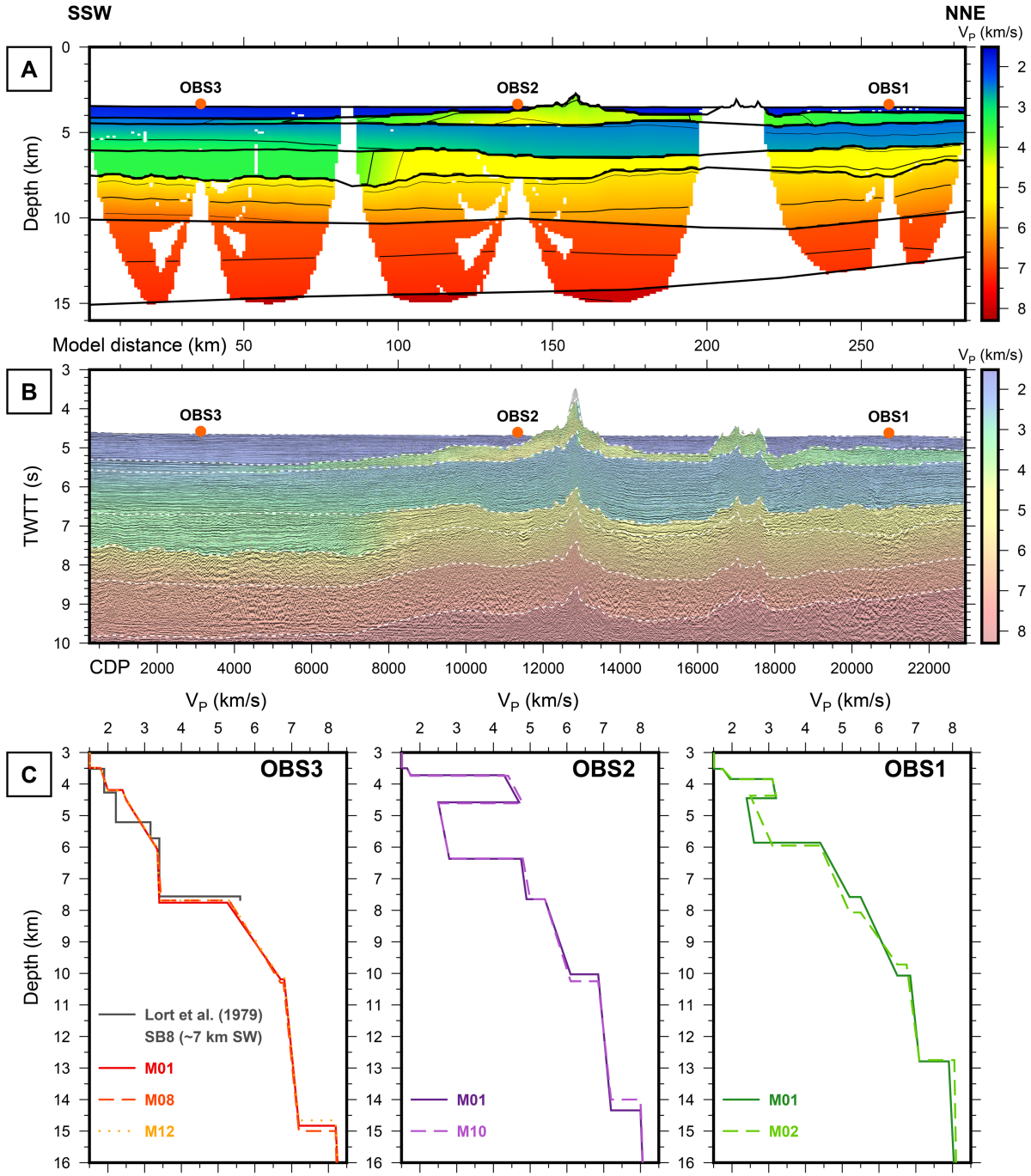

Figure 2: Results of the OBS data analysis. A: Velocity model along the M01 profile. B: Seismic reflection data overlaid on the time-converted velocity model. C: Vertical velocity profiles beneath each OBS for each crossing shot line.

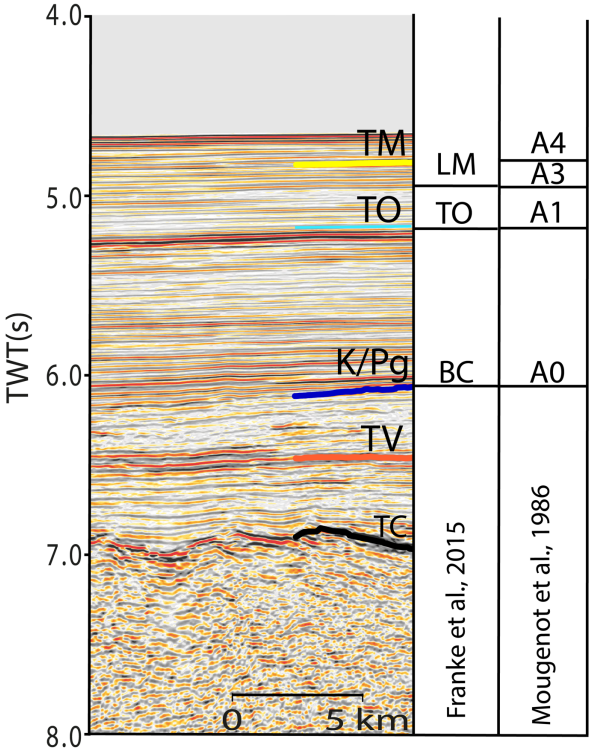

Figure 3: Seismic stratigraphy of the Comoros Basin from Masquelet et al. (submitted). The seismic character of the interpreted key horizons is illustrated by a 960-channel seismic reflection profile; the Top Miocene (TM; 5.3 Ma), Top Oligocene (TO; 23.5 Ma), Cretaceous-Paleogene unconformity (K/Pg; 66 Ma), Turonian volcanism (TV; 89-93 Ma), and the top of the crust were identified in the Comoros Basin and compared with the seismic stratigraphy of Franke et al. (2015) and Mougenot et al. (1986): BC/A0: Cretaceous/Tertiary boundary; TO/A1: Top Oligocene; LM/A3: Late Miocene; A4: Pliocene.

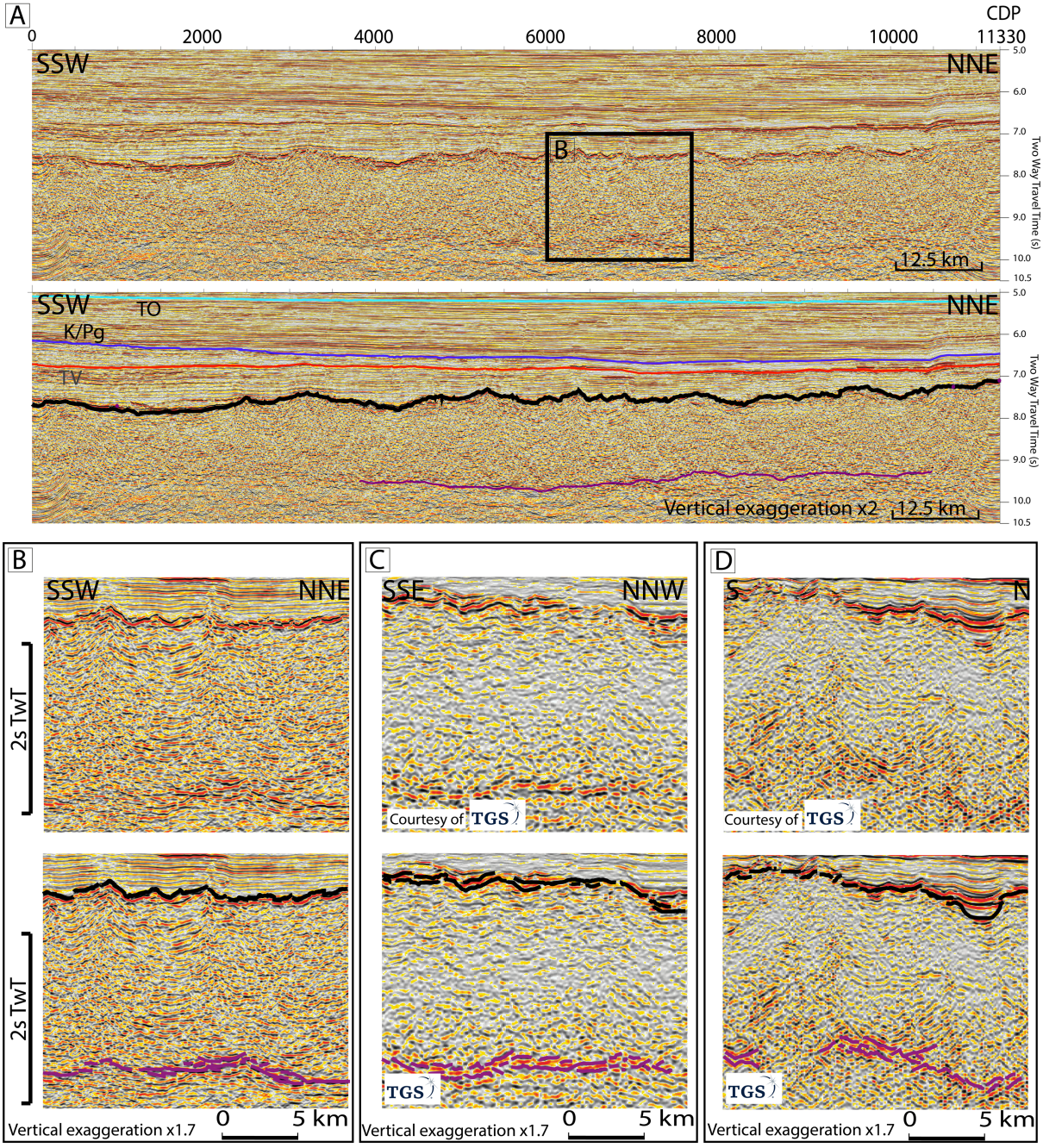

569

570 **Figure 4**: M09 960-channel seismic reflection profile east of Mayotte (A), and
571 interpreted profile (see location in Fig. 1). The black and purple lines correspond to the
572 top of the crust and the Moho, respectively. TO: Top Oligocene. K/Pg:
573 Cretaceous/Paleogene boundary, TV: Turonian volcanism. (B) Close-up view of part
574 of the M09 profile location shown in (A). (C) and (D) show other examples of typical
575 oceanic crust (see location of the profiles in Fig.1).

576

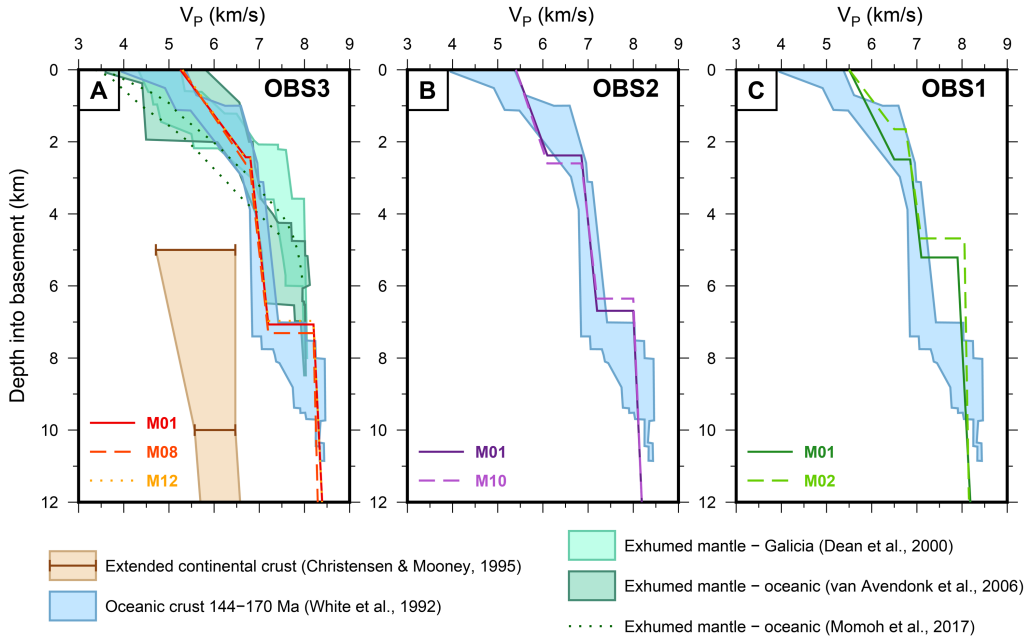

577

578 **Figure 5**: Vertical velocity profiles in the basement and uppermost mantle for OBS3
579 (A), OBS2 (B) and OBS3 (C), compared with literature data for oceanic crust, extended
580 continental crust, sub-continental exhumed mantle and oceanic exhumed mantle.

581

582

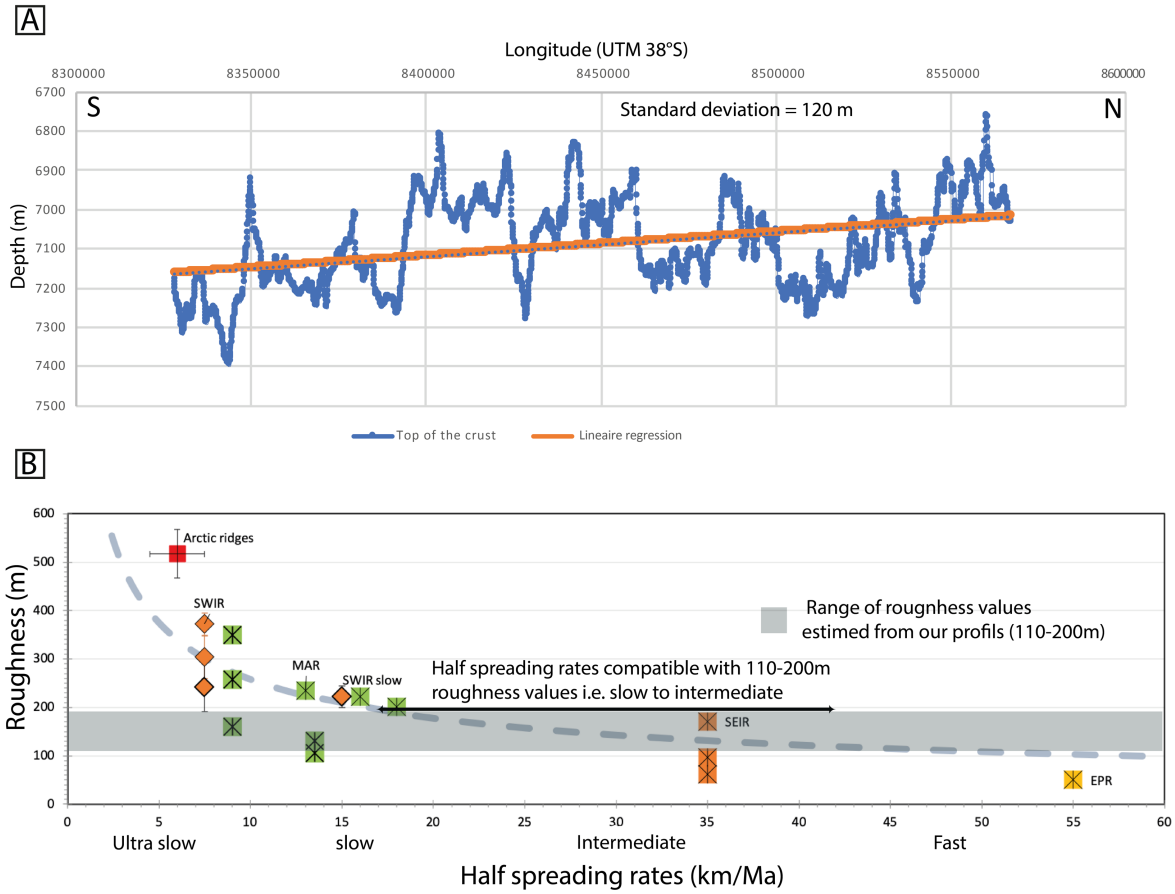

Figure 6: Roughness estimate for a NS profile in the Comoros Basin (A; see location in Fig. 1) and plot of the roughness versus spreading rate (B). Depth values were obtained by converting TWTT using the velocity profile of OBS3. The standard deviation of the detrended profile in A gives a roughness value of 120 m. Roughness values for the Artic Ridge are from Weigelt and Jokat (2001) and Ehlers and Jokat (2009). Those for the southwest Indian ultraslow-spreading ridge are from Sloan et al. (2012). Those for the slow-spreading Mid-Atlantic Ridge are from Goff (1991); Goff et al. (1997); Minshull (1999); Neumann and Forsyth (1995). The roughness value for the slow-spreading SWIR (before 24 Ma) is from Sauter et al. (2011). The roughness values for the intermediate-spreading southeast Indian Ridge and fast-spreading East Pacific Rise are from Goff et al. (1997). The dashed grey line is the power-law curve fit of Malinverno (1991). The horizontal grey box shows the range of roughness values measured in our study area.

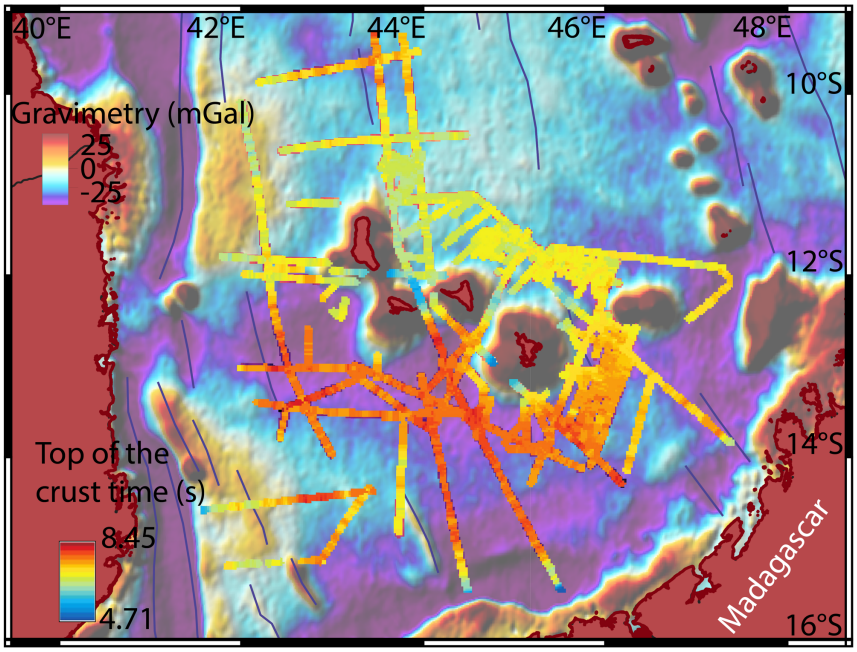

Figure 7: Depth of the top of the crust (in seconds two-way travel time) obtained along the seismic reflection profiles. The blue lines correspond to the fracture zones from Davis et al. (2016). The background image is the satellite-derived free-air gravity anomaly grid of Sandwell et al. (2014).

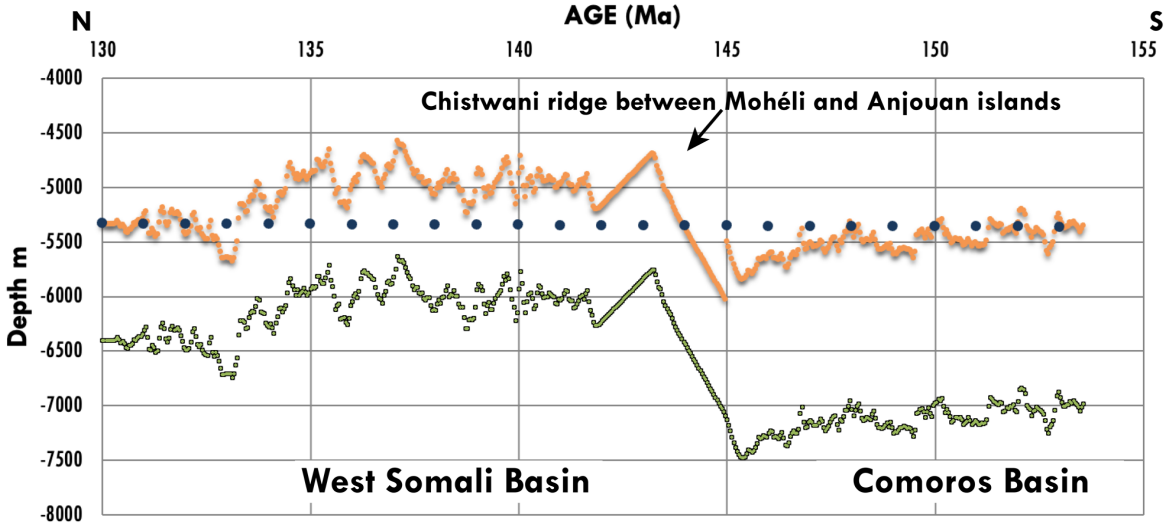

609

610 **Figure 8**: Depth of the top basement obtained along a NS seismic reflection located
611 at 44°E longitude and passing between the islands of Anjouan and Mohéli (green dots)
612 (Figs 1 and 7 for location). Black dots follow the GDH1 cooling model of Stein and
613 Stein (1992) for a standard oceanic lithosphere. Orange dots show the depth of the
614 basement free from the weight of the sediments. Ages are calculated using the
615 distance from the extinct axis and an intermediate 25 km/Ma half spreading rate.

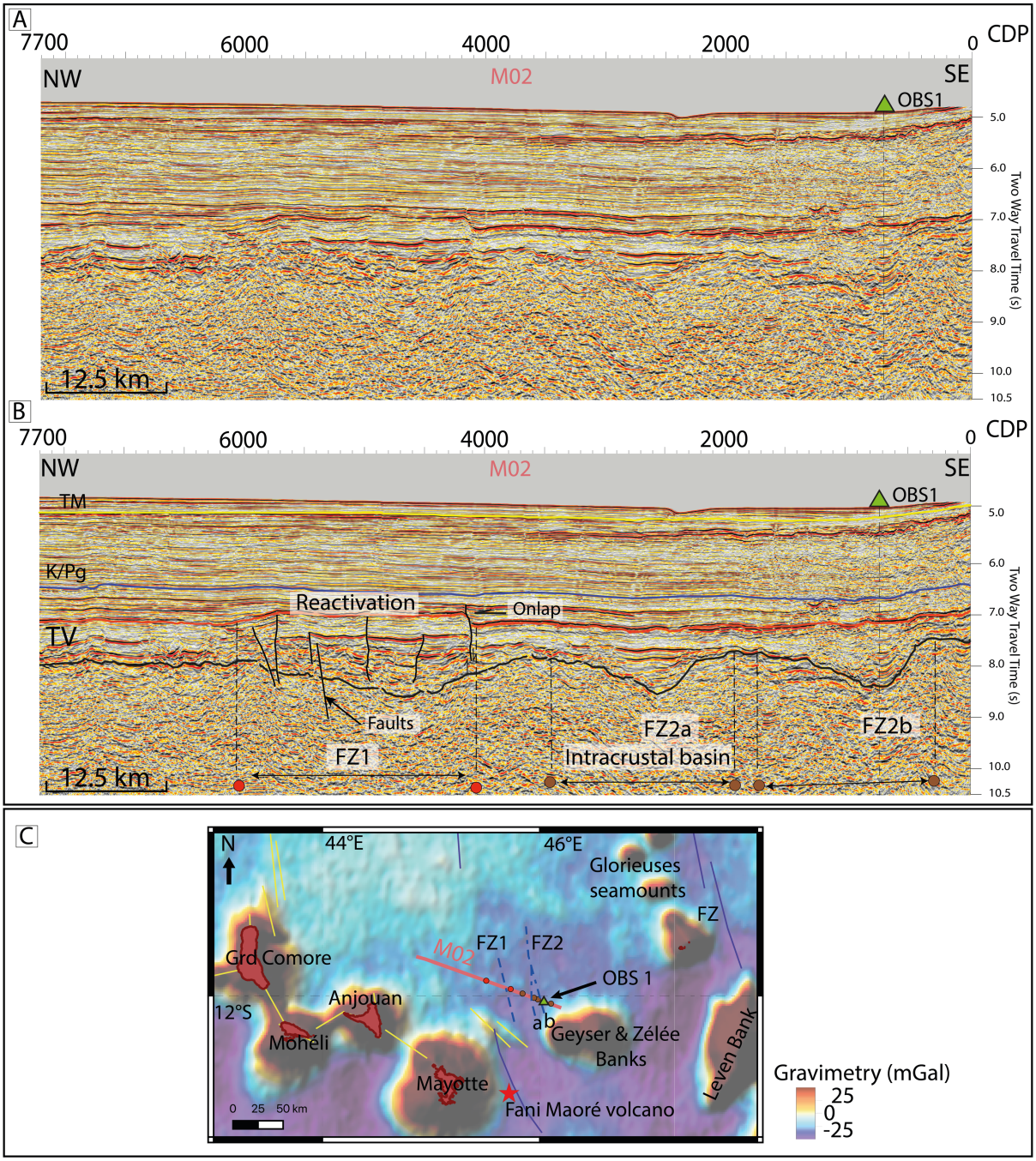

Figure 9: M02 960-channel seismic reflection profile north of Mayotte (A), interpreted profile (B) and location map (C). TM: Top Miocene; K/Pg: Cretaceous-Paleogene boundary; TV: Turonian Volcanism. In frame C, the dashed blue lines indicate the location of inferred fracture zones (FZ1 & FZ2) using the seismic profiles M01 and M02. The background image is the satellite-derived free-air gravity anomaly grid of Sandwell et al. (2014). Blue lines correspond to the fracture zones (FZ) mapped by Davis et al. (2016). Yellow thick lines show the main orientations of some volcanic structures.

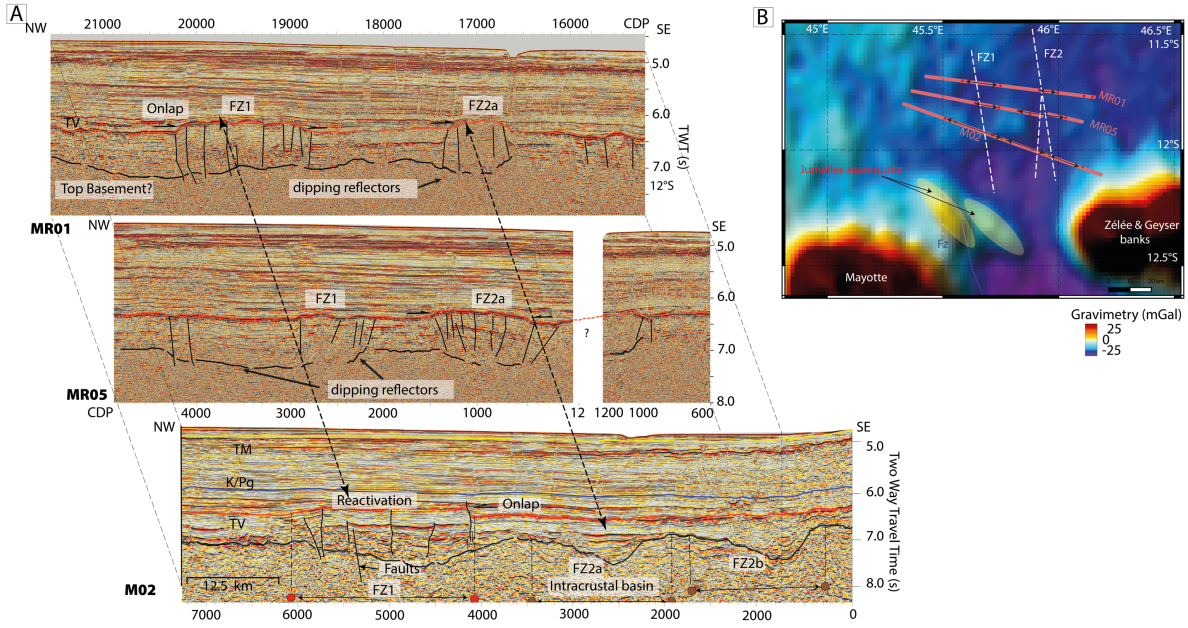

Figure 10: Identification of reactivated fracture zones (Fz1, Fz2a, Fz2b) observed on three EW-trending seismic reflection profiles (A) and location map with fracture zones shown as white dashed lines (B). The dipping reflectors (black lines) in the 48-channel seismic reflection profiles (MR05 and MR01) are interpreted as the top of the oceanic crust.

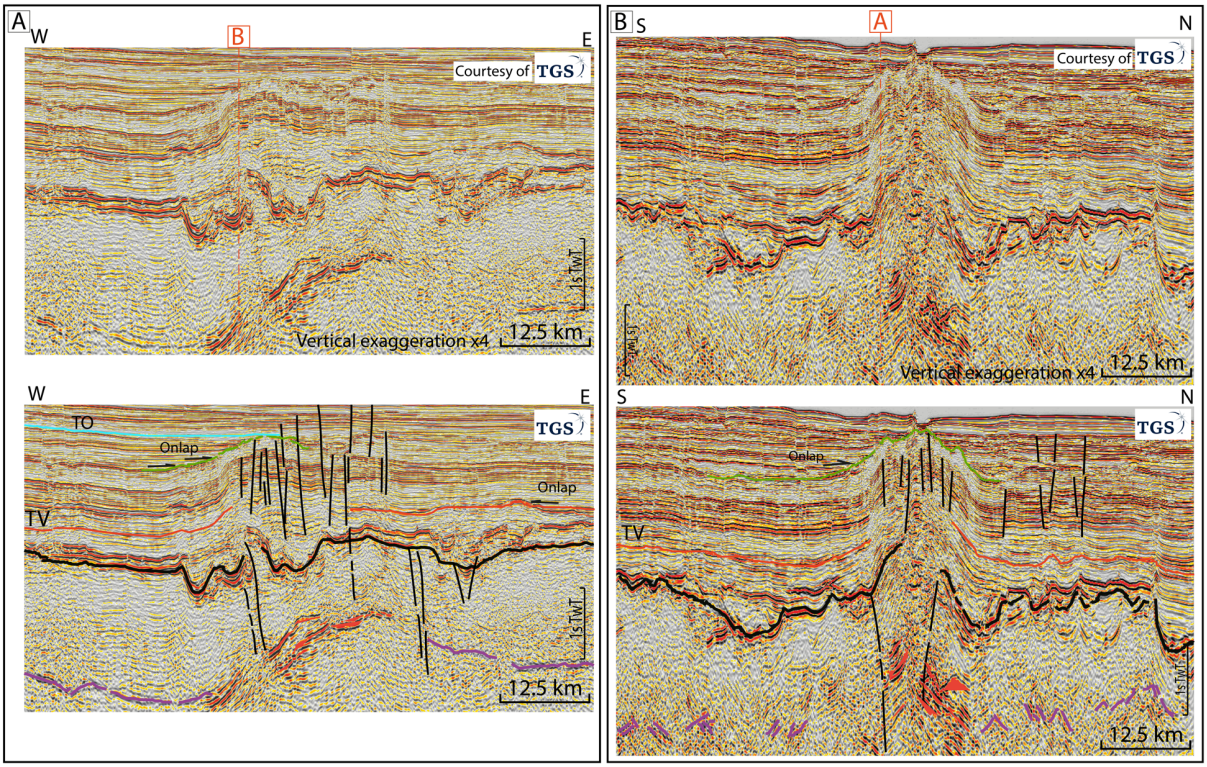

Figure 11: Sections of an EW-trending seismic reflection profile (A) and an NS-trending seismic reflection profile (B) north of the Grande Comore Island (see location in Fig. 1). TO: Top Oligocene, TV: Turonian Volcanism. The green horizon shows the last sedimentary layer affected by the compressional deformation. The thick black and purple lines correspond to the top of the oceanic crust and the Moho, respectively. The thin black lines indicate faults.

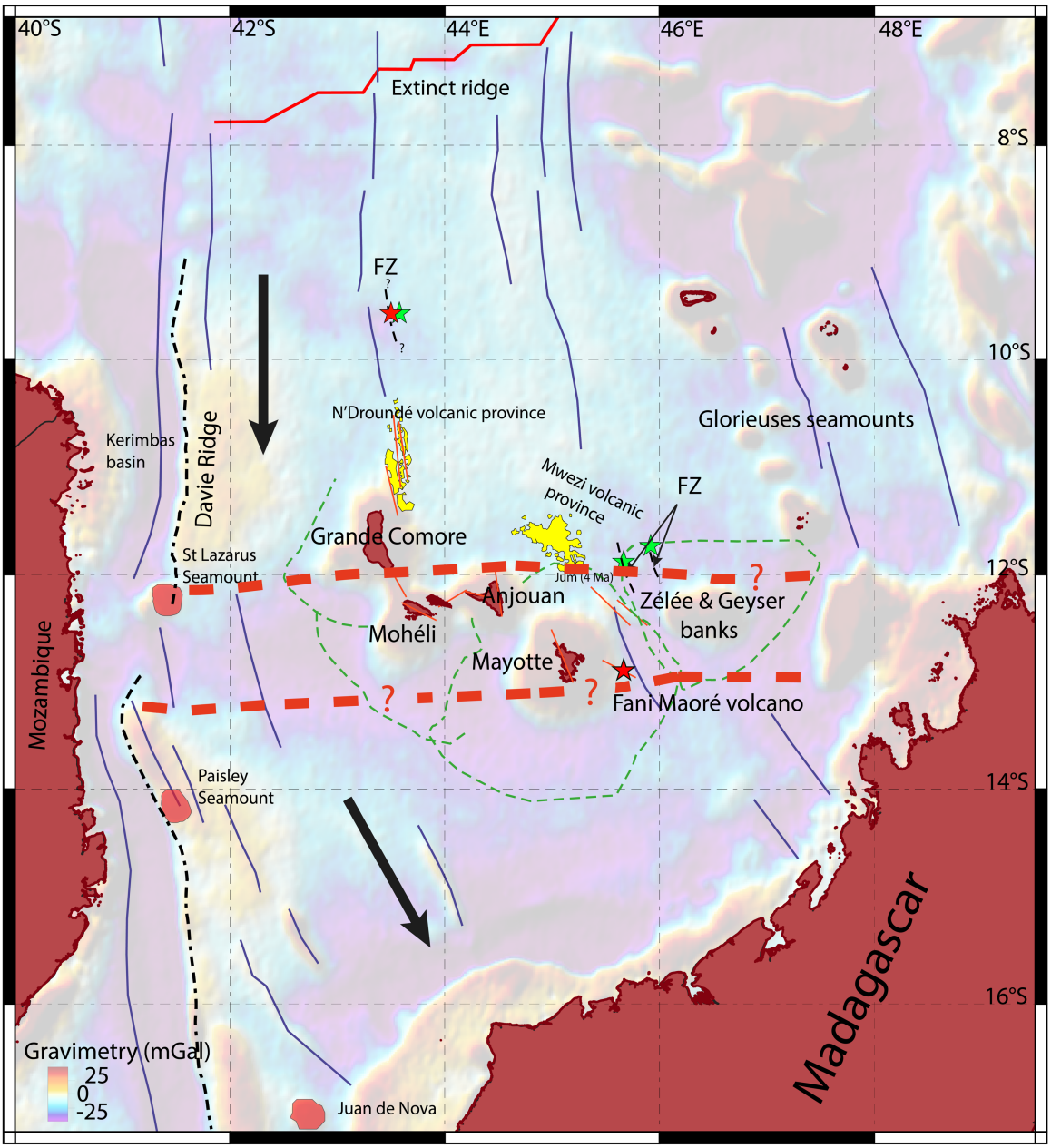

Figure 12: Schematic structural map of the West Somali and Comoros Basins. The black arrows show the paleo-spreading direction. The thin red line corresponds to the location of the extinct spreading ridge. The black dashed line corresponds to the location of Davie Ridge. The blue lines are the fracture zones identified by Davis et al., (2016). The dashed green lines indicate the extent of the volcanic zones around each island (Masquelet et al., submitted). The dashed red lines delimit the area where the fracture zones show a marked change in direction. The stars indicate the location of the reactivated fracture zones shown in Figs 9-11. The background image is the satellite-derived free-air gravity anomaly grid of Sandwell et al. (2014).

REFERENCES CITED

Altenbernd, T., Jokat, W., Geissler, W., 2020. The bent prolongation of the 85°E Ridge south of 5°N – Fact or fiction? Tectonophysics 785, 228457. https://doi.org/10.1016/j.tecto.2020.228457

Bassias, Y., Leclaire, L., 1990. The Davie Ridge in the Mozambique Channel: Crystalline basement and intraplate magmatism. njgpm 1990, 67–90. https://doi.org/10.1127/njgpm/1990/1990/67

Bécel, A., Shillington, D.J., Nedimović, M.R., Webb, S.C., Kuehn, H., 2015. Origin of dipping structures in fast-spreading oceanic lower crust offshore Alaska imaged by multichannel seismic data. Earth and Planetary Science Letters 424, 26–37. https://doi.org/10.1016/j.epsl.2015.05.016

Christensen, N.I., Mooney, W.D., 1995. Seismic velocity structure and composition of the continental crust: A global view. J. Geophys. Res. 100, 9761–9788. https://doi.org/10.1029/95JB00259

Christeson, G.L., Goff, J.A., Reece, R.S., 2019. Synthesis of Oceanic Crustal Structure From Two-Dimensional Seismic Profiles. Reviews of Geophysics 57, 504–529. https://doi.org/10.1029/2019RG000641

Class, C., Goldstein, S.L., Shirey, S.B., 2009. Osmium isotopes in Grande Comore lavas: A new extreme among a spectrum of EM-type mantle endmembers. Earth and Planetary Science Letters 284, 219–227. https://doi.org/10.1016/j.epsl.2009.04.031

Cochran, J.R., 1988. Somali Basin, Chain Ridge, and origin of the Northern Somali Basin gravity and geoid low. J. Geophys. Res. 93, 11985. https://doi.org/10.1029/JB093iB10p11985

Coffin, M.F., Rabinowitz, P.D., 1992. The Mesozoic East African and Madagascan Conjugate Continental MarginsStratigraphy and Tectonics, in: Geology and Geophysics of Continental Margins. American Association of Petroleum Geologists. https://doi.org/10.1306/M53552C12

Coffin, M.F., Rabinowitz, P.D., Houtz, R.E., 1986. Crustal structure in the Western Somali Basin. Geophysical Journal International 86, 331–369. https://doi.org/10.1111/j.1365-246X.1986.tb03832.x

Collins, J.A., Brocher, T.M., Karson, J.A., 1986. Two-dimensional seismic reflection modeling of the inferred fossil oceanic crust/mantle transition in the Bay of Islands Ophiolite. J. Geophys. Res. 91, 12520–12538. https://doi.org/10.1029/JB091iB12p12520

Cruciani, F., Barchi, M.R., 2016. The Lamu Basin deepwater fold-and-thrust belt: An example of a margin-scale, gravity-driven thrust belt along the continental passive margin of East Africa: the Lamu basin DW-FTB. Tectonics 35, 491–510. https://doi.org/10.1002/2015TC003856

Davis, J.K., Lawver, L.A., Norton, I.O., Gahagan, L.M., 2016. New Somali Basin magnetic anomalies and a plate model for the early Indian Ocean. Gondwana Research 34, 16–28. https://doi.org/10.1016/j.gr.2016.02.010

Dean, S.M., Minshull, T.A., Whitmarsh, R.B., Louden, K.E., 2000. Deep structure of the ocean-continent transition in the southern Iberia Abyssal Plain from seismic refraction profiles: The IAM-9 transect at 40°20′N. J. Geophys. Res. 105, 5859–5885. https://doi.org/10.1029/1999JB900301

Dofal, A., Fontaine, F.R., Michon, L., Barruol, G., Tkalčić, H., 2021. Nature of the crust beneath the islands of the Mozambique Channel: Constraints from

receiver functions. Journal of African Earth Sciences 184, 104379. https://doi.org/10.1016/j.jafrearsci.2021.104379
Dofal, A., Michon, L., Fontaine, F.R., Rindraharisaona, E., Barruol, G., Tkalčić, H., 2023. Imaging the lithospheric structure and plumbing system below the Mayotte volcanic zone. Comptes Rendus. Géoscience 354, 47–64. https://doi.org/10.5802/crgeos.190
Ehlers, B.-M., Jokat, W., 2009. Subsidence and crustal roughness of ultra-slow spreading ridges in the northern North Atlantic and the Arctic Ocean. Geophysical Journal International 177, 451–462. https://doi.org/10.1111/j.1365-246X.2009.04078.x
Emerick, C.M., Duncan, R.A., 1982. Age progressive volcanism in the Comores Archipelago, western Indian Ocean and implications for Somali plate tectonics. Earth and Planetary Science Letters 60, 415–428. https://doi.org/10.1016/0012-821X(82)90077-2
Famin, V., Michon, L., Bourhane, A., 2020. The Comoros archipelago: a right-lateral transform boundary between the Somalia and Lwandle plates. Tectonophysics 789, 228539. https://doi.org/10.1016/j.tecto.2020.228539
Feuillet, N., Jorry, S., Crawford, W.C., Deplus, C., Thinon, I., Jacques, E., Saurel, J.M., Lemoine, A., Paquet, F., Satriano, C., Aiken, C., Foix, O., Kowalski, P., Laurent, A., Rinnert, E., Cathalot, C., Donval, J.-P., Guyader, V., Gaillot, A., Scalabrin, C., Moreira, M., Peltier, A., Beauducel, F., Grandin, R., Ballu, V., Daniel, R., Pelleau, P., Gomez, J., Besançon, S., Geli, L., Bernard, P., Bachelery, P., Fouquet, Y., Bertil, D., Lemarchand, A., Van der Woerd, J., 2021. Birth of a large volcanic edifice offshore Mayotte via lithosphere-scale dyke intrusion. Nat. Geosci. 14, 787–795. https://doi.org/10.1038/s41561-021-00809-x
Flower, M.F.J., Strong, D.F., 1969. The significance of sandstone inclusions in lavas of the comores archipelago. Earth and Planetary Science Letters 7, 47–50. https://doi.org/10.1016/0012-821X(69)90010-7
Foulger, G.R., Doré, T., Emeleus, C.H., Franke, D., Geoffroy, L., Gernigon, L., Hey, R., Holdsworth, R.E., Hole, M., Höskuldsson, Á., Julian, B., Kusznir, N., Martinez, F., McCaffrey, K.J.W., Natland, J.H., Peace, A.L., Petersen, K., Schiffer, C., Stephenson, R., Stoker, M., 2020. The Iceland Microcontinent and a continental Greenland-Iceland-Faroe Ridge. Earth-Science Reviews 206, 102926. https://doi.org/10.1016/j.earscirev.2019.102926
Franke, D., Jokat, W., Ladage, S., Stollhofen, H., Klimke, J., Lutz, R., Mahanjane, E.S., Ehrhardt, A., Schreckenberger, B., 2015. The offshore East African Rift System: Structural framework at the toe of a juvenile rift: the offshore East African Rift. Tectonics 34, 2086–2104. https://doi.org/10.1002/2015TC003922
Goff, J.A., 1991. A global and regional stochastic analysis of near-ridge Abyssal Hill morphology. J. Geophys. Res. 96, 21713–21737. https://doi.org/10.1029/91JB02275
Goff, J.A., Ma, Y., Shah, A., Cochran, J.R., Sempéré, J., 1997. Stochastic analysis of seafloor morphology on the flank of the Southeast Indian Ridge: The influence of ridge morphology on the formation of abyssal hills. J. Geophys. Res. 102, 15521–15534. https://doi.org/10.1029/97JB00781
Hajash, A., Armstrong, R.L., 1972. Paleomagnetic and radiometric evidence for the age of the Comores Islands, west central Indian Ocean. Earth and Planetary Science Letters 16, 231–236. https://doi.org/10.1016/0012-821X(72)90195-1
Hall, I.R., Hemming, S.R., LeVay, L.J., Scientists, E. 361, 2017. South African

752 Climates (Agulhas LGM Density Profile). Proceedings of the International
753 Ocean Discovery Program 361. https://doi.org/10.14379/iodp.proc.361.2017
754 Jorry, S., 2014. PTOLEMEE cruise,L'Atalante R/V.
755 https://doi.org/10.17600/14000900
756 Klimke, J., Franke, D., Gaedicke, C., Schreckenberger, B., Schnabel, M., Stollhofen,
757 H., Rose, J., Chaheire, M., 2016. How to identify oceanic crust—Evidence for
758 a complex break-up in the Mozambique Channel, off East Africa.
759 Tectonophysics 693, 436–452. https://doi.org/10.1016/j.tecto.2015.10.012
760 Lemoine, A., Briole, P., Bertil, D., Roullé, A., Foumelis, M., Thinon, I., Raucoules, D.,
761 de Michele, M., Valty, P., Hoste Colomer, R., 2020. The 2018–2019 seismo-
762 volcanic crisis east of Mayotte, Comoros islands: seismicity and ground
763 deformation markers of an exceptional submarine eruption. Geophysical
764 Journal International 223, 22–44. https://doi.org/10.1093/gji/ggaa273
765 Leroux, E., Counts, J.W., Jorry, S.J., Jouet, G., Révillon, S., BouDagher-Fadel, M.K.,
766 Courgeon, S., Berthod, C., Ruffet, G., Bachèlery, P., Grenard-Grand, E., 2020.
767 Evolution of the Glorieuses seamount in the SW Indian Ocean and
768 surrounding deep Somali Basin since the Cretaceous. Marine Geology 427,
769 106202. https://doi.org/10.1016/j.margeo.2020.106202
770 Lort, J.M., Limond, W.Q., Segoufin, J., Patriat, Ph., Delteil, J.R., Damotte, B., 1979.
771 New seismic data in the Mozambique Channel. Mar Geophys Res 4, 71–89.
772 https://doi.org/10.1007/BF00286146
773 Mahanjane, E.S., 2014. The Davie Fracture Zone and adjacent basins in the offshore
774 Mozambique Margin - A new insights for the hydrocarbon potential. Marine
775 and Petroleum Geology 11.
776 Malinverno, A., 1991. Inverse square-root dependence of mid-ocean-ridge flank
777 roughness on spreading rate. Nature 352, 58–60.
778 https://doi.org/10.1038/352058a0
779 Mascle, J., Mougenot, D., Blarez, E., Marinho, M., Virlogeux, P., 1987. African
780 transform continental margins: Examples from Guinea, the Ivory Coast and
781 Mozambique. Geol. J. 22, 537–561. https://doi.org/10.1002/gj.3350220632
782 Masquelet, C., Leroy, S., Chamot-Rooke, N., Thinon, I., Lemoine, A., Franke, D.,
783 Watremez, L., Werner, P., Paquet, F., Berthod, C., Cabiativa Pico, V., Sauter,
784 D., 2022. The East-Mayotte new volcano in the Comoros Archipelago:
785 structure and timing of magmatic phases inferred from seismic reflection data.
786 Comptes Rendus. Géoscience Tome 354, 65–79. https://doi.org/doi :
787 10.5802/crgeos.154.
788 Masquelet, C., Sauter, D., Leroy, S., Delescluse, M., Chamot-Rooke, N., Thinon, I.,
789 Watremez, L., Lemoine, A., Franke, D., Zaragosi, S., Ringenbach, J.C.,
790 Beaufort, L., submitted. The Comoros Archipelago, Madagascar and the East
791 African Rift System: what is the link? Earth Planet. Sci. Lett.
792 Michon, L., Famin, V., Quidelleur, X., 2022. Evolution of the East African Rift System
793 from trap-scale to plate-scale rifting. Earth-Science Reviews 231, 104089.
794 https://doi.org/10.1016/j.earscirev.2022.104089
795 Minshull, T.A., 1999. On the roughness of Mesozoic oceanic crust in the western
796 North Atlantic. Geophysical Journal International 136, 286–290.
797 https://doi.org/10.1046/j.1365-246X.1999.00722.x
798 Minshull, T.A., Muller, M.R., White, R.S., 2006. Crustal structure of the Southwest
799 Indian Ridge at 66°E: seismic constraints. Geophysical Journal International
800 166, 135–147. https://doi.org/10.1111/j.1365-246X.2006.03001.x
801 Montaggioni, L.F., Nougier, J., 1981. Les enclaves de roches detritiques dans les

802 Volcans d'Anjouan (Archipel des Comores); Origine et interpretation dans le
803 cadre de l'evolution du Canal de Mozambique. Bulletin de la Société
804 Géologique de France S7-XXIII, 595–601.
805 https://doi.org/10.2113/gssgfbull.S7-XXIII.6.595
806 Morgan, W.J., Morgan, J.P., 2007. Plate velocities in the hotspot reference frame, in:
807 Special Paper 430: Plates, Plumes and Planetary Processes. Geological
808 Society of America, pp. 65–78. https://doi.org/10.1130/2007.2430(04)
809 Mougenot, D., Recq, M., Virlogeux, P., Lepvrier, C., 1986. Seaward extension of the
810 East African Rift. Nature 321, 599–603. https://doi.org/10.1038/321599a0
811 Mutter, J.C., Carton, H.D., 2013. The Mohorovicic discontinuity in ocean basins:
812 Some observations from seismic data. Tectonophysics 609, 314–330.
813 https://doi.org/10.1016/j.tecto.2013.02.018
814 Neumann, G.A., Forsyth, D.W., 1995. High resolution statistical estimation of seafloor
815 morphology: Oblique and orthogonal fabric on the flanks of the Mid-Atlantic
816 Ridge, 34°-35.5° S. Mar Geophys Res 17, 221–250.
817 https://doi.org/10.1007/BF01203464
818 Nougier, J., Cantagrel, J.M., Karche, J.P., 1986. The Comores archipelago in the
819 western Indian Ocean: volcanology, geochronology and geodynamic setting.
820 Journal of African Earth Sciences (1983) 5, 135–145.
821 https://doi.org/10.1016/0899-5362(86)90003-5
822 Ogg, J.G., 2020. Geomagnetic Polarity Time Scale, in: Geologic Time Scale 2020.
823 Elsevier, pp. 159–192. https://doi.org/10.1016/B978-0-12-824360-2.00005-X
824 Péron-Pinvidic, G., Manatschal, G., 2010. From microcontinents to extensional
825 allochthons: witnesses of how continents rift and break apart? PG 16, 189–
826 197. https://doi.org/10.1144/1354-079309-903
827 Phethean, J.J.J., Kalnins, L.M., van Hunen, J., Biffi, P.G., Davies, R.J., McCaffrey,
828 K.J.W., 2016. Madagascar's escape from Africa: A high-resolution plate
829 reconstruction for the Western Somali Basin and implications for
830 supercontinent dispersal: MADAGASCAR'S ESCAPE FROM AFRICA.
831 Geochem. Geophys. Geosyst. 17, 5036–5055.
832 https://doi.org/10.1002/2016GC006624
833 Quidelleur, X., Michon, L., Famin, V., Geffray, M.-C., Danišík, M., Gardiner, N.,
834 Rusquet, A., Zakaria, M.G., 2022. Holocene volcanic activity in Anjouan Island
835 (Comoros archipelago) revealed by new Cassignol-Gillot groundmass K–Ar
836 and 14C ages. Quaternary Geochronology 67, 101236.
837 https://doi.org/10.1016/j.quageo.2021.101236
838 Rabinowitz, P.D., Coffin, M.F., Falvey, D., 1983. The Separation of Madagascar and
839 Africa. Science 220, 67–69. https://doi.org/10.1126/science.220.4592.67
840 Razafindrazaka, Y., Randriamananjara, T., Piqué, A., Thouin, C., Laville, E., Malod,
841 J., Réhault, J.-P., 1999. Extension et sédimentation au paléozoïque terminal
842 et au Mésozoïque dans le bassin de Majunga (Nord-Ouest de Madagascar).
843 Journal of African Earth Sciences 28, 949–959. https://doi.org/10.1016/S0899-
844 5362(99)00071-8
845 Reeves, C.V., 2018. The development of the East African margin during Jurassic and
846 Lower Cretaceous times: a perspective from global tectonics. Petroleum
847 Geoscience 24, 41–56. https://doi.org/10.1144/petgeo2017-021
848 Roche, V., Ringenbach, J.-C., 2022. The Davie Fracture Zone: A recorder of
849 continents drifts and kinematic changes. Tectonophysics 823, 229188.
850 https://doi.org/10.1016/j.tecto.2021.229188
851 Rusquet, A., Famin, V., Quidelleur, X., Michon, L., Nauret, F., Danišík, M., Thinon, I.,

Leroy, S., Lemoine, A., 2023. Pliocene-to-Holocene volcano-tectonic activity on Mohéli Island (Comoros archipelago) constrained by new K Ar ages. Journal of Volcanology and Geothermal Research 442, 107896. https://doi.org/10.1016/j.jvolgeores.2023.107896

Sandwell, D.T., Müller, R.D., Smith, W.H.F., Garcia, E., Francis, R., 2014. New global marine gravity model from CryoSat-2 and Jason-1 reveals buried tectonic structure. Science 346, 65–67. https://doi.org/10.1126/science.1258213

Sauter, D., Ringenbach, J.C., Cannat, M., Maurin, T., Manatschal, G., McDermott, K.G., 2018a. Intraplate Deformation of Oceanic Crust in the West Somali Basin: Insights From Long-offset Reflection Seismic Data. Tectonics 37, 588–603. https://doi.org/10.1002/2017TC004700

Sauter, D., Sloan, H., Cannat, M., Goff, J., Patriat, P., Schaming, M., Roest, W.R., 2011. From slow to ultra-slow: How does spreading rate affect seafloor roughness and crustal thickness? Geology 39, 911–914. https://doi.org/10.1130/G32028.1

Sauter, D., Tugend, J., Gillard, M., Nirrengarten, M., Autin, J., Manatschal, G., Cannat, M., Leroy, S., Schaming, M., 2018b. Oceanic basement roughness alongside magma-poor rifted margins: insight into initial seafloor spreading. Geophysical Journal International 212, 900–915. https://doi.org/10.1093/gji/ggx439

Sauter, D., Unternehr, P., Manatschal, G., Tugend, J., Cannat, M., Le Quellec, P., Kusznir, N., Munschy, M., Leroy, S., Mercier De Lepinay, J., Granath, J.W., Horn, B.W., 2016. Evidence for magma entrapment below oceanic crust from deep seismic reflections in the Western Somali Basin. Geology 44, 407–410. https://doi.org/10.1130/G37747.1

Sauter, D., Werner, P., Ceuleneer, G., Manatschal, G., Rospabé, M., Tugend, J., Gillard, M., Autin, J., Ulrich, M., 2021. Sub-axial deformation in oceanic lower crust: Insights from seismic reflection profiles in the Enderby Basin and comparison with the Oman ophiolite. Earth and Planetary Science Letters 554, 116698. https://doi.org/10.1016/j.epsl.2020.116698

Ségoufin, J., Patriat, P., 1980. Existence d'anomalies mesozoiques dans le basin de Somalie. Implications pour les relations Afrique- Antarctique-Madagascar. Comptes Rendus de l' Académie des Sciences Série IIa:Sciences de la Terre et des Planètes 85–88.

Simpson, E.S.W., Schlich, R., et al., 1974. Initial Reports of the Deep Sea Drilling Project, 25, Initial Reports of the Deep Sea Drilling Project. U.S. Government Printing Office. https://doi.org/10.2973/dsdp.proc.25.1974

Sinha, S.T., Saha, S., Longacre, M., Basu, S., Jha, R., Mondal, T., 2019. Crustal Architecture and Nature of Continental Breakup Along a Transform Margin: New Insights From Tanzania-Mozambique Margin. Tectonics 38, 1273–1291. https://doi.org/10.1029/2018TC005221

Sloan, H., Sauter, D., Goff, J.A., Cannat, M., 2012. Abyssal hill characterization at the ultraslow spreading Southwest Indian Ridge. Geochem Geophys Geosyst 13, 2011GC003850. https://doi.org/10.1029/2011GC003850

Song, P., Ding, L., Zhang, L., Cai, F., Zhang, Q., Li, Z., Wang, H., Jafari, M.K., Talebian, M., 2023. Paleomagnetism From Central Iran Reveals Arabia-Eurasia Collision Onset at the Eocene/Oligocene Boundary. Geophysical Research Letters 50, e2023GL103858. https://doi.org/10.1029/2023GL103858

Stamps, D.S., Kreemer, C., Fernandes, R., Rajaonarison, T.A., Rambolamanana, G.,

2021. Redefining East African Rift System kinematics. Geology 49, 150–155. https://doi.org/10.1130/G47985.1

Stein, C.A., Stein, S., 1992. A model for the global variation in oceanic depth and heat flow with lithospheric age. Nature 359, 123–129. https://doi.org/10.1038/359123a0

Thinon, I., Lemoine, A., Leroy, S., Paquet, F., Berthod, C., Zaragosi, S., Famin, V., Feuillet, N., Boymond, P., Masquelet, C., Mercury, N., Rusquet, A., Scalabrin, C., Van der Woerd, J., Bernard, J., Bignon, J., Clouard, V., Doubre, C., Jacques, E., Jorry, S.J., Rolandone, F., Chamot-Rooke, N., Delescluse, M., Franke, D., Watremez, L., Bachèlery, P., Michon, L., Sauter, D., Bujan, S., Canva, A., Dassie, E., Roche, V., Ali, S., Sitti Allaouia, A.H., Deplus, C., Rad, S., Sadeski, L., 2022. Volcanism and tectonics unveiled in the Comoros Archipelago between Africa and Madagascar. Comptes Rendus. Géoscience 354, 1–28. https://doi.org/10.5802/crgeos.159

Thinon, I., Leroy, S., Lemoine, A., 2020. SISMAORE cruise, RV Pourquoi pas ?,. https://doi.org/10.17600/18001331

Tzevahirtzian, A., Zaragosi, S., Bachèlery, P., Biscara, L., Marchès, E., 2021. Submarine morphology of the Comoros volcanic archipelago. Marine Geology 432, 106383. https://doi.org/10.1016/j.margeo.2020.106383

Van Avendonk, H.J.A., Holbrook, W.S., Nunes, G.T., Shillington, D.J., Tucholke, B.E., Louden, K.E., Larsen, H.C., Hopper, J.R., 2006. Seismic velocity structure of the rifted margin of the eastern Grand Banks of Newfoundland, Canada. J. Geophys. Res. 111, 2005JB004156. https://doi.org/10.1029/2005JB004156

Van Der Zwan, F.M., Augustin, N., Le Saout, M., Seidel, E., Wölfl, A.-C., Schade, M., Lampridou, D., Long, X., Follmann, J., Miluch, J., Schönberg, J., Antonio, R.J., Heinath, V., Köse, M.C., Krach, L., Garbe-Schönberg, C.-D., Hübscher, C., 2023. Tectonically assisted emplacement of oceanic intraplate volcanoes: The Bathymetrists Seamounts, central Atlantic. Geomorphology 441, 108891. https://doi.org/10.1016/j.geomorph.2023.108891

Vormann, M., Franke, D., Jokat, W., 2020. The crustal structure of the southern Davie Ridge offshore northern Mozambique – A wide-angle seismic and potential field study. Tectonophysics 778, 228370. https://doi.org/10.1016/j.tecto.2020.228370

Vormann, M., Jokat, W., 2021. Crustal variability along the rifted/sheared East African margin: a review. Geo-Mar Lett 41, 19. https://doi.org/10.1007/s00367-021-00690-y

Weigelt, E., Jokat, W., 2001. Peculiarities of roughness and thickness of oceanic crust in the Eurasian Basin, Arctic Ocean. Geophysical Journal International 145, 505–516. https://doi.org/10.1046/j.1365-246X.2001.00398.x

White, R.S., McKenzie, D., O'Nions, R.K., 1992. Oceanic crustal thickness from seismic measurements and rare earth element inversions. J. Geophys. Res. 97, 19683–19715. https://doi.org/10.1029/92JB01749

Zelt, C.A., Smith, R.B., 1992. Seismic traveltime inversion for 2-D crustal velocity structure. Geophysical Journal International 108, 16–34. https://doi.org/10.1111/j.1365-246X.1992.tb00836.x